Molecular Mechanism of Surface-Assisted Epitaxial Self-Assembly of Amyloid-like Peptides

Seung-gu Kang,[†] Hai Li,[‡] Tien Huynh,[†] Fuchun Zhang,[‡] Zhen Xia,[†,§] Yi Zhang,[‡,*] and Ruhong Zhou[†,⊥,*]

[†]Computational Biology Center, IBM Thomas J. Watson Research Center, Yorktown Heights, New York 10598, United States, [‡]Shanghai Institute of Applied Physics, Chinese Academy of Sciences, Shanghai 201800, China, [§]Department of Biomedical Engineering, The University of Texas at Austin, Austin, Texas 78712, United States, and [⊥]Department of Chemistry, Columbia University, New York, New York 10027, United States

ABSTRACT

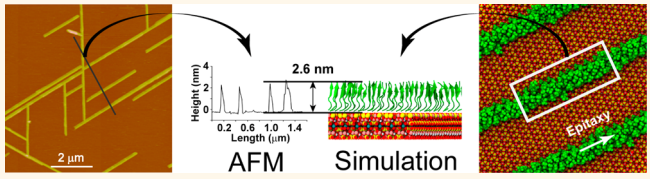

A surprising "upright" fibrilar conformation (with a height of ~2.6 nm) was observed with *in situ* atomic force microscopy (AFM) for an amyloid-like peptide (NH_2-VGGAVVAV-$COHN_2$) on mica surface, which is very different from its "flat" conformation (with a much smaller height of ~0.9 nm) on the HOPG surface. Our all-atom molecular dynamics (MD) simulations reveal that it is the strong electrostatic interactions between the N-terminus of the peptide and the mica surface that result in an upright conformation and a highly ordered β-stranded structure on mica, with a height of 2.5 ± 0.1 nm, consistent with the AFM experiment. Similarly, our MD simulations show that the same peptides adopt a flat conformation on HOPG surfaces due to the favorable hydrophobic interactions with HOPG. Our simulations also indicate that epitaxial patterns found in mica are preferentially controlled by anisotropic binding sites commensurate with the inherent crystallographic unit cell of the basal substrate.

KEYWORDS: peptide self-assembly · muscovite mica · epitaxial growth · amyloid peptide · molecular dynamics simulation

Self-assembly of amyloid-like peptides on substrate surfaces has motivated great interest lately due to their pathological implications on amylodosis[1−3] and potential applications in *de novo* nanodevice design and fabrication.[4] Various factors modulate the complexity of peptide amyloidogenesis on the solid surfaces, including peptide sequence, peptide concentration, pH value, ionic strength, temperature, solvent, surface polarity, and so on. Among these, the supporting substrate often controls morphology of the adsorbed assembly as the most significant factor. For example, amyloid-β peptide (Aβ), a peptide associated with Alzheimer disease, formed oligomeric protofibrilar aggregates on mica, whereas it assembled along the surface epitaxial order on a highly oriented pyrolytic graphite (HOPG) surface, forming elongated structures.[5,6] By contrast, α-synuclein (α-syn), a pathogenic protein in Parkinson's disease, showed sheet growth along the crystalline atomic structure of the mica surface but not on the hydrophobic HOPG.[7] While the substrate−peptide interaction is generally accepted as a critical factor for peptide assembly,[8,9] the molecular level understanding of how the substrate structure affects the peptide assembly structure and growth epitaxy still remains elusive.

Recently, we reported self-assembly of an amyloid-related peptide motif, GAV-9 (NH_2-VGGAVVAGV-$CONH_2$),[10] obtained from consensus sequences from the Aβ peptide, α-syn, and prion protein (PrP).[11] The *in situ* atomic force microscopy (AFM) showed epitaxial growth of GAV-9 on both polar mica and nonpolar HOPG, however, with different morphologies. In this study, we used a simplified version, P4 (NH_2-VGGAVVAV-$CONH_2$) with the residue Gly_8 deletion from GAV-9. Using *in situ* AFM and all-atom molecular dynamics (MD) simulations, we examined the difference of the assembly on mica and HOPG, the substrate effect on the assembly, and underling driving forces.

RESULTS AND DISCUSSION

Peptide Self-Assembly on Polar and Nonpolar Surfaces. Figure 1 shows the self-assembly of the P4 peptides on mica and HOPG surfaces obtained by *in situ* AFM imaging. P4 peptides clearly form linearly assembled nanostructures on both surfaces. They assembled preferentially along three orientations at 120° to each other, consistently reflecting the hexagonal atomic lattice of the basal substrate. This can be explained by the

* Address correspondence to ruhongz@us.ibm.com, zhangyi@sinap.ac.cn.

Received for review August 16, 2012 and accepted September 24, 2012.

Published online September 24, 2012
10.1021/nn303740j

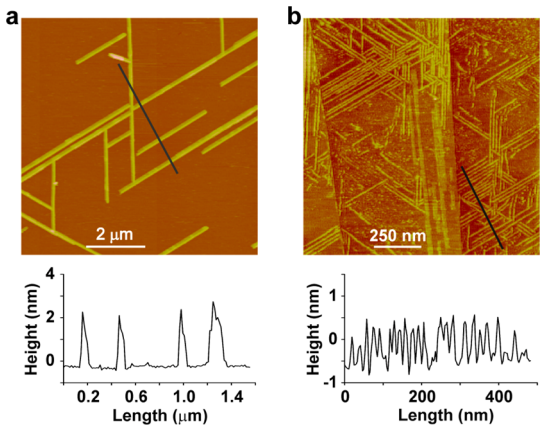

Figure 1. AFM image of self-assembled nanofilaments of P4 peptides on mica and graphite surfaces. (a) Epitaxial assembly on muscovite (001) surface and section analysis on the line marked in black. (b) Epitaxial growth on HOPG surface and section analysis on the line marked in black.

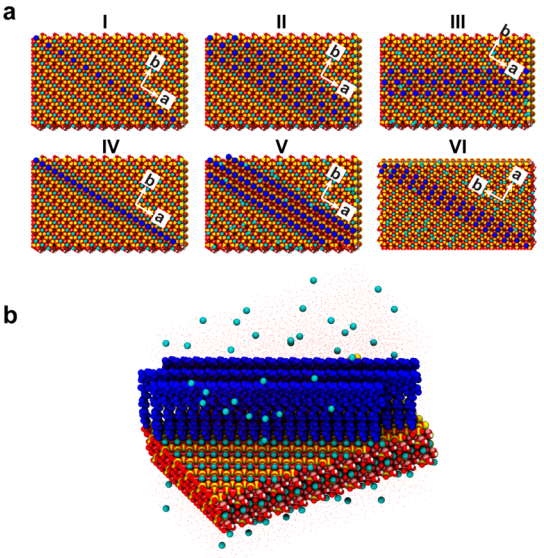

Figure 2. Six configurations in molecular dynamics simulations. (a) P4 peptides are loaded on the mica surface depending on surface density, supporting rows, and epitaxial direction, where the blue dots display position of the N-terminal nitrogen atoms of P4 peptides. Two arrows with letters in each setup indicate two anisotropic epitaxial binding directions (*i.e.*, *a*- and *b*-directions). (b) Perspective view of starting structure of configuration V, where three peptide rows (blue) are loaded on mica along the longitudinal *a*-direction. Dots colored with cyan in the solvent are counterions to neutralize the system.

substrate-assisted one-dimensional epitaxial growth process found in other examples.[7,12,13]

Despite apparent similarities in the epitaxial growth on both surfaces, the heights of the peptide nanostructures differ, with 2.6 ± 0.2 nm on mica and 0.9 ± 0.1 nm on HOPG. This proposes distinctive models for peptides on two different surfaces. Interestingly, the height on mica is comparable with the length scale of ~2.8 nm when P4 is in its fully extended state (based on the 0.695 nm between two repeating C_α carbons of a β-sheet[14]). Meanwhile, the height on HOPG matches with the width of ~1 nm of typical β-strands.[15] Indeed, on mica, P4 peptides stand up to assemble by facilitating electrostatic interaction between the positive N-termini of peptides and negative surface charges, while on HOPG, the peptides lie down *via* hydrophobic interactions between P4 side chains and the surface.

The similar epitaxial pattern was also observed with GAV-9 peptides on both surfaces,[10] however, with a higher critical concentration (1.6 mM on mica) than P4 (1.0 mM on mica) for the assembly initiation. The difference in critical concentration could be related to a decrease in the peptide mainchain's degree of freedom due to the deletion of residue Gly_8 in P4. The AFM section analysis showed a similar height trend of ~1.0 nm on HOPG and ~3.0 nm on mica,[10] again consistent with the width and length dimensions of the peptide in the extended conformation, suggesting similar assembly mechanism as the P4 peptide. The slightly larger height of GAV-9 on mica is due to one additional glycine residue on site 8.

Surface Polarity Intrinsically Controls the Assembly of the Hydrophobic P4 Peptides. Next, we attempt to understand possible assembly dynamics of P4 peptides on mica and HOPG using all-atom molecular dynamics simulations. The mica surface was constructed with double-layered muscovite (001) ($KAl_2(Si_3Al)O_{10}(OH)_2$) with the CLAYFF force field,[16] and the HOPG was prepared with four layers of graphene sheets (Figure S1 in the Supporting Information). On the mica surface, two different epitaxial directions exist depending on the distance between the nearest epitaxial binding sites (centers of Al/Si ditrigonal six-membered tetrahedral rings): short (d_a = 0.52 nm) and long (d_b = 0.92 nm) distanced epitaxial binding sites along with the shorter (*a*-direction) and longer (*b*-direction) crystallographic unit cell directions, respectively. Each direction repeats every 120°.[17] Due to the lack of structural information on the assembly on mica, various possible assembly patterns were investigated by examining six different configurations (conf-I−VI) starting from reasonably small number of peptides, ranging from 12 to 72 chains depending on packing density and assembly direction with visual inspections on the mica surface (Figure 2a). The peptide packing densities increase in the order of **I** = **II** < **III** < **IV** = **V** = **VI** (see detailed rationales below and in the Supporting Information).

Figure 3 shows the snapshot at the end of the MD simulation. In the low-density conf-I and conf-II, P4 peptides are generally stable at their initially deposited sites on mica except one or two chains. The peptide positioning is largely attributed to favorable electrostatic interactions between the positive N-terminal NH^{3+} and the negatively charged muscovite surface, as validated in high cation exchange capacity of NH^{3+} on K-mica.[18,19] Interestingly, even in the low-concentration conf-I, peptides on mica can stand up with an

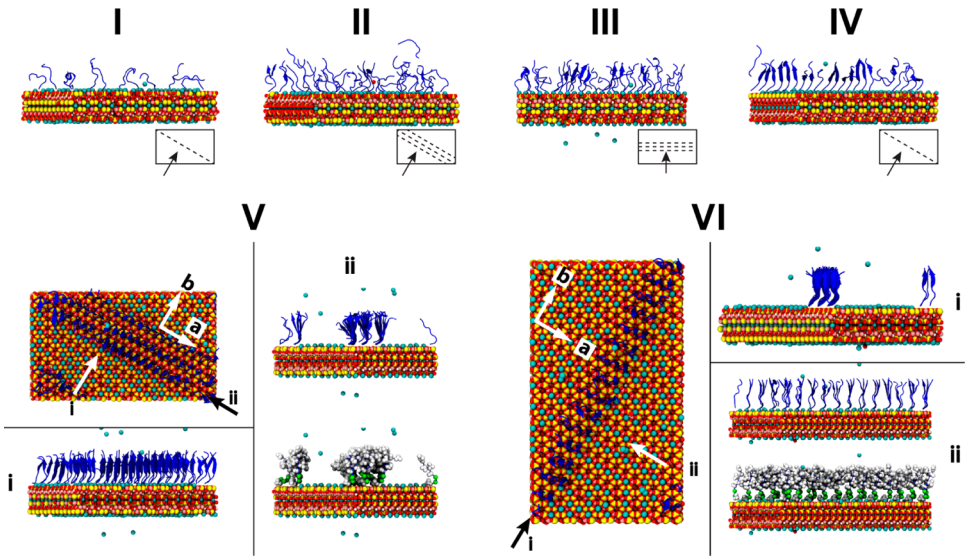

Figure 3. Representative structures from molecular dynamics simulation after ~100 ns. Even in low-density configurations (I–III), peptides tend to stand up on mica in more or less random-coiled states with transient and local secondary structures. In tightly packed cases (IV–VI), however, the long-range β-strands are dominantly formed. The conf-V and VI show that P4 peptides form stable hydrogen bonding networks (see viewpoint through i) and hydrophobic interactions (see viewpoint ii) along the *a*-direction and *b*-direction, respectively, where the hydrophobic residues are depicted with white space-filling models.

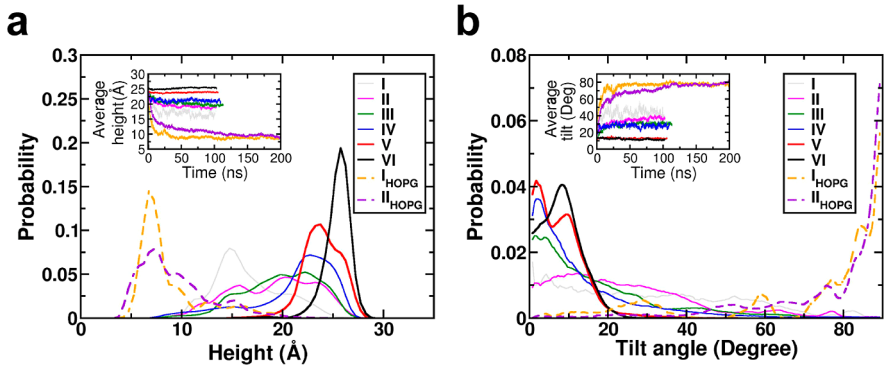

Figure 4. Average heights and tilting angles of P4 peptides. (a) Height distribution of P4 peptides, where the height is defined as a peptide length projected onto the axis of the surface normal, and time profiles of peptide heights averaged over all chains in each time frame (inset). The conf-VI on mica has a height of ~2.5 nm, consistent with the AFM section analysis value (~2.6 nm). (b) Tilting angle distribution of P4 peptides, where the tilt angle is defined as the angle difference between the principal axis of a peptide and the surface normal, and time profiles on peptide tilting angles averaged over all chains (inset). The peptides on mica tend to erect on mica with only ~8° tilted from the surface normal (*i.e.*, conf-VI), but they quickly lie down on HOPG. The distributions are normalized with a sinusoidal distribution function.

average peptide height of 1.6 ± 0.3 nm and tilt angle of 30 ± 21° from the surface normal (Figure 4), while the hydrophobic tails move freely in water in a random coiled state. This is distinctly contrasted with the result of similar density on HOPG (I_{HOPG}), where almost all P4 peptides completely lie down on the surface from the upright position within 50 ns, resulting in an average height <1.0 nm and a tilt angle of ~90° from the surface normal (Figures 4 and S2). The same also happens to the tightly packed peptides on HOPG (II_{HOPG}) but with a slight delay on the collapse. The low-density results are qualitatively consistent with the experimental observation of "standing-up" on mica and "lying-down" on HOPG, implying that the surface polarity is one of the intrinsic factors controlling the peptide assembly. Indeed, considering that the P4 only has hydrophobic side chains, it would be energetically favorable to lie down on the hydrophobic HOPG to maximize the hydrophobic interactions, whereas the negative charges on mica and its hydrophilic water layers would avoid the adsorption of the hydrophobic side chains to it. Water molecules are also shown to form a highly ordered two-dimensional ice-like structure in both experiments[20,21] and theory,[22] which is confirmed in our current simulations (results shown in Figure S3). These findings suggest a molecular mechanism of greater enthalpy loss than entropy gain when hydrophobic molecules absorb onto and desolvate the mica surface.

P4 Assembly on Mica Is Controlled by Surface Density and Growth Direction. Despite the qualitative agreement, the

low-density result is not sufficient to explain the quantitative behavior found in the AFM on mica (*i.e.*, 2.6 nm in height). In our next sets of simulations, we added supporting rows (conf-II) as well as slightly increased peptide density (conf-III). However, this was not fully satisfactory as both assisted only slightly for the peptides to stand up with a height and tilt angle of ~1.9 nm, ~25° and ~2.0 nm, ~17° as seen in conf-II and conf-III, respectively (Figure 4). However, one thing interesting to notice is that they start to make secondary structures, albeit existing only transiently and locally. This inspires us to construct even tighter packed structures (*i.e.*, conf-IV, conf-V, and conf-VI).

In conf-IV, peptides were placed on every possible (*i.e.*, nearest neighbor) epitaxial site along the *a*-direction, which initially we chose to omit due to the extremely tight dimension match between the peptide width (~1 nm) and the binding site separation ($d_a \approx$ 0.5 nm), but it turned out that the peptides can be accommodated by stretching out their bulky hydrophobic side chains toward the less crowed side line (*i.e.*, *b*-direction), thus leaving only backbone atoms along the longitudinal axis of the assembly line (*i.e.*, *a*-direction). This resulted in a ~2.1 nm height and ~13° tilt angle, even with no supporting rows (Figure 3IV). However, this arrangement may cause energetically unfavorable processes, such as sequestration of the hydrophilic backbone atoms from water and exposure of the hydrophobic side chains to water. The former could be compensated by the intermolecular hydrogen bond as shown in the global enhancement of the secondary structures (Figure 3IV), and the latter could be resolved by additional rows (detailed discussion below).

On the basis of this finding, we examine the effects of the two additional factors: (1) supporting multirows (V) along the growth direction (instead of monorow in IV), and (2) growing along the other perpendicular direction (*b*-direction; VI). The configuration V has two nearest neighboring parallel supporting rows away from the central monorow (by the unit distance d_b = 0.92 nm). Our simulation shows a dramatic enhancement in their structural integrity, where almost all peptides are involved in the long-range β-stranded structure from the very early stage of simulations even though it started with arbitrary elongated conformation (Figure 3V), resulting in a tilt angle of ~8° and a height of ~2.4 nm. With regard to the assembly growth direction, we also examined the growth along the *b*-direction (conf-VI) with the same density as conf-V. The result was remarkably consistent with the experiment, with an average height of 2.5 ± 0.1 nm. Even with a similar tilt angle (~8°) as in conf-V, the peptides in the conf-VI tend to stand up straighter (as shown in Rg of Figure 4S) with much narrower and regular height distribution (Figure 4).

In the tightly packed systems V and VI, the P4 peptides are able to construct an efficient hydrogen bond network along the *a*-direction through polar backbone atoms (Figure 5a), as shown in conf-IV. At the same time, the bulky hydrophobic side chains make a favorable knob-and-hole type of van der Waals interactions through the *b*-direction as to bury each other from the solvent (Figure 5b), which makes more stable β-structures than the monorowed conf-IV. The following analyses (Figure 5c,d) on backbone dihedral angles and hydrogen bonds summarize the interplay between peptide density and their structural integrity. That is, peptides are more ordered with increasing stable β-strands in the tightly packed configurations (*i.e.*, IV−VI), while in the loosely packed configurations, they are more likely to be in random coils (*i.e.*, I−III). This finding indicates how the substrate structure affects the peptide self-assembly, intertwined with intrinsic interpeptide interactions.[23] It is noteworthy that the ordered self-assembly on mica is largely attributed to lattice matching between the two-dimensional anisotropies of the mica surface and the β-stranded peptide network, where the interpeptide hydrogen bond distance (~0.48 nm) and the face-to-face distance (~1 nm) of peptide β-structure fit almost perfectly with the mica anisotropic binding sites along the *a*-direction (~0.5 nm) and *b*-direction (~0.9 nm), respectively.[24] This explains how the mica surface helps to register peptides in epitaxial adsorption and acts as a catalyst in the highly ordered structural formation as proposed in other examples with the surface-assisted epitaxial growth.[7−9,12,13]

Our result also implies that the *b*-directional growth shown in the conf-VI seems more plausible. Although peptides in the core of the conf-V and conf-VI may have similar interactions with neighboring chains and the mica surface, the peptides in the outside edge are in a slightly different environment, which in turn will be critical in determining the assembly growth direction. Indeed, in the edge of conf-V, the hydrophobic side chains are exposed to water, whereas, in conf-VI, it is the polar backbone atoms that are exposed to water. This provides an important clue to unmask the assembly growth mechanism. The exposed hydrophobic edge would be more reactive with the incoming peptides, similar to hydrophobic collapses in the protein folding.[6,25−27] By contrast, peptides approaching the open hydrophilic edge would be less favorable due to relatively high desolvation energies for removing hydration shells formed near the hydrophilic backbone.[23] Overall, these facts will help favor the longitudinal growth along the epitaxial *b*-direction of the mica surface rather than the *a*-direction, which is in good agreement with the AFM observation.

To conclude, we observed a linear assembled pattern of an amyloid-related eight-residue P4 peptide on the polar mica and nonpolar HOPG surfaces. While they made similar epitaxial patterns, the AFM section analysis implied very different assembly structures and dynamics on the two surfaces. From our molecular

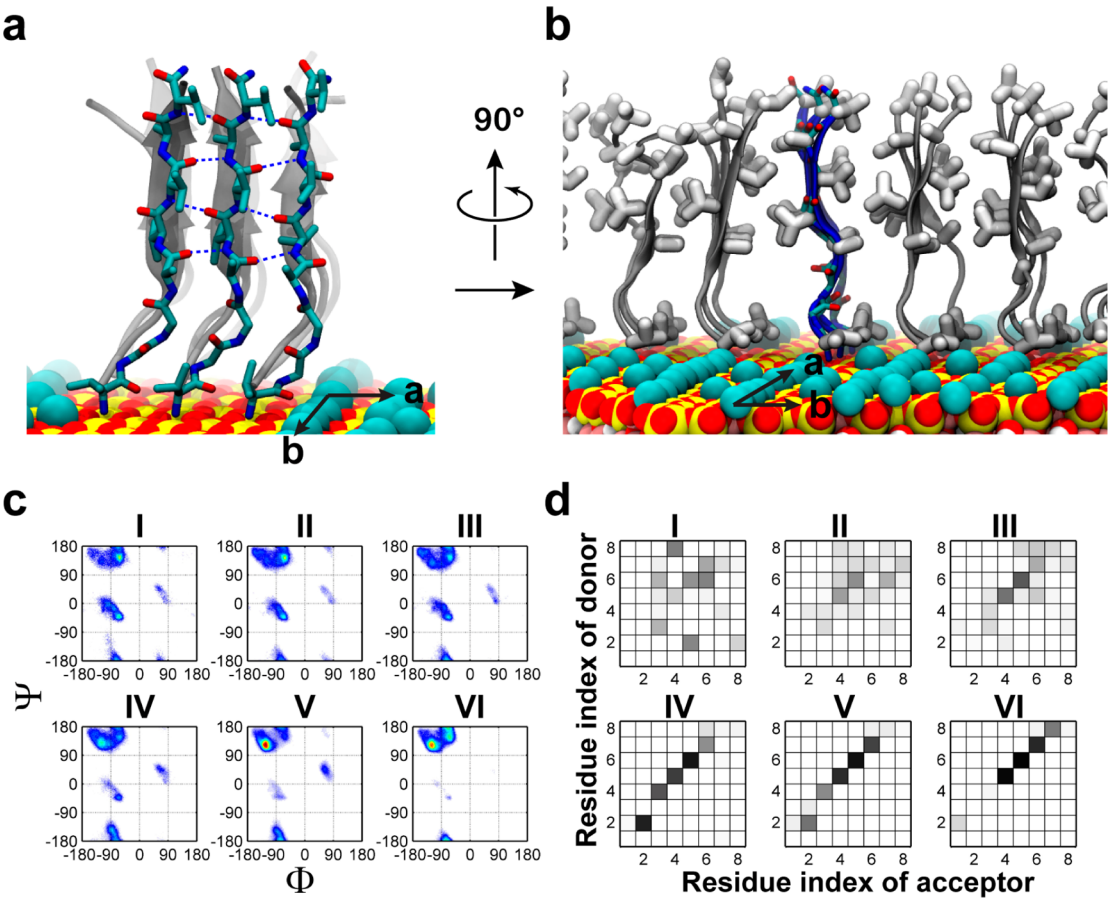

Figure 5. Substrate incorporation for formation of a highly ordered epitaxial assembly of P4 peptides on mica. (a) Hydrogen bonding network following the short-distanced epitaxial *a*-direction of mica surface. (b) Knob-and-hole type hydrophobic interaction along the long-distanced epitaxial *b*-direction of mica, where the hydrophobic side chains are depicted with white sticks. (c) Ramachandran plots. As surface density increases, the β-structures become significantly dominant (*i.e.*, see population on top-left corner), where color spans from white to red to indicate low and high probabilities, respectively. (d) Interpeptide hydrogen bonding network. As surface density increases, the backbone hydrogen bonds between residues of side chains become more probable, resulting in highly ordered β-stranded structures, where color spans from white to black to indicate low and high probabilities, respectively.

dynamics simulations, we revealed that the surface polarity can be a more crucial factor in determining the peptide assembly process than the properties of the adsorbent peptide. In the detailed study on mica, we further revealed key factors affecting the assembly, including surface anisotropy, peptide density, and interpeptide interactions. In one configuration (conf-VI), we obtained remarkable consistence with the AFM-measured height of 2.6 $\pm$ 0.2 nm. Our simulations demonstrate how the muscovite (001) mica could serve as a catalytic template for the highly ordered peptide self-assembly formation. The anisotropy of the mica surface (*i.e.*, two epitaxial binding sites along shorter (*a*-direction) and longer (*b*-direction) unit cell vectors) facilitates interpeptide backbone hydrogen bonds along the short-distanced epitaxial *a*-direction as well as side chain hydrophobic interactions along the long-distanced (longitudinal) *b*-direction, giving rise to a stable long-range β-stranded peptide network. This further proposes a potential mechanism about the epitaxial growth on mica, a growth along the *b*-direction *via* a more reactive hydrophobic edge. Our results provide detailed insight into the surface-assisted self-assembly on the molecular level, especially the underling factors for the epitaxial growth on mica. It would be an important guide for *de novo* two-dimensional nanopatterning as well as pathogenic amyloid-like peptide aggregation.

MATERIALS AND METHODS

P4 Peptide and AFM. The peptide, NH_2-VGGAVVAV-$CONH_2$, was synthesized by using the Boc solid-phase method on an ABI 433 A peptide synthesizer (Applied Biosystems) and then purified with a TSK-40 (S) column (2.0 cm $\times$ 98 cm, Tosoh). Before its usage, the peptide powder was dissolved in PBS buffer (10 mmol/L phosphate, 10 mmol/L NaCl, pH 7.0). Muscovite mica (Sichuan Meifeng Co., China) and highly ordered pyrolytic graphite (HOPG, grade ZYB, MikroMasch Co., Russia) were used as the substrates for peptide assembly, which were freshly

cleaved by adhesive tape prior to each experiment. Peptide filaments were formed by placing a drop of an aqueous solution of the peptide on the substrates as previously reported.[10,28] The peptide concentrations were set at 1.0 mM and 20 μM for assembly on mica and HOPG, respectively. *In situ* imaging of the assembling peptide filaments on substrates was performed on a commercial atomic force microscope (AFM, Nanoscope IIIa, Veeco/Digital Instruments, USA) equipped with a J-scanner. All AFM measurements were carried out with tapping mode in liquid. Silicon nitride cantilevers with a nominal spring constant of 0.22 N/m (NPS, Veeco/Digital Instruments) were used.

Molecular Dynamics Simulations. The mica surface was constructed with double-layered muscovite (001) ($KAl_2(Si_3Al)O_{10}(OH)_2$) with the CLAYFF force field[16] based on the monoclinic $C2/c2M_1$ crystal structure[17] according to the Loewenstein Al avoidance rule.[29,30] The HOPG was prepared with four layers of graphene sheets using the CHARMM22 force field.[31] As mentioned in the main text, we configured six different systems (conf-I−VI) on the mica surface depending on surface density, supporting rows and growth direction (Figure 2a). Both conf-I and conf-II have the same linear densities, but conf-II has two supporting rows with 12 peptides aligned in each row along the *a*-direction in every alternative epitaxial binding site. The linear packing density is increased in conf-III by arranging the same number of peptides as conf-II (*i.e.*, 36 chains) along the *x*-axis (*i.e.*, *b*-direction) of the same size of mica surface instead of the diagonal direction with loosely packed supporting rows. From conf-IV, the peptides are more tightly packed along the *a*-direction by placing 24 peptides in every possible epitaxial binding site, resulting in density doubling that of conf-I. The conf-V (72 peptides) and conf-VI (48 peptides) have the same surface densities as conf-IV but are in different growth directions. A 107.6 $\times$ 63.8 Å^2 muscovite for conf-I−V and a 71.8 $\times$ 127.7 Å^2 surface for conf-VI are used to ensure linear assembly over the periodic boundary condition. As controls, two cases of low (I_{HOPG}; 12 peptides) and high (II_{HOPG}; 24 peptides) densities were prepared on a 109.5 $\times$ 65.5 Å^2 HOPG surface (Figure S1). Then, the system was solvated with ~12 000 TIP3P[32] water molecules. All molecular dynamics simulations were done with the NAMD software[33] specially parallelized on the IBM Bluegene computer.[34] The long-range electrostatic interactions were enumerated with the particle mesh Ewald method.[35] The nonbonding dispersion energies were considered for atoms within 12.0 Å. Each system was first optimized in 20 000 steps and equilibrated in 0.5 ns with a 0.5 fs time step in the NPT ensemble at 1 atm and 310 K. Production runs were performed with a 2 fs time step for at least 100 ns duration on mica and 200 ns on HOPG.

Conflict of Interest: The authors declare no competing financial interest.

Acknowledgment. We would like to thank Bruce J. Berne, Haiping Fang, Guanghong Wei, and Jun Hu for helpful discussions. We also thank Royce W. Zhou, Matteo Castelli, and Raul Araya for critical reading of the manuscript. Y.Z. thanks the National Science Foundation of China for support of a grant (No. 10975175).

Supporting Information Available: P4 peptide assemblies on HOPG surface, ordered water structure on mica surface, and Rg of P4 peptides in different configurations. This material is available free of charge *via* the Internet at http://pubs.acs.org.

REFERENCES AND NOTES

1. Murphy, R. M. Kinetics of Amyloid Formation and Membrane Interaction with Amyloidogenic Proteins. *Biochim. Biophys. Acta* **2007**, *1768*, 1923–1934.
2. Butterfield, S. M.; Lashuel, H. A. Amyloidogenic Protein−Membrane Interactions: Mechanistic Insight from Model Systems. *Angew. Chem., Int. Ed.* **2010**, *49*, 5628–5654.
3. Chiti, F.; Dobson, C. M. Protein Misfolding, Functional Amyloid, and Human Disease. *Annu. Rev. Biochem.* **2006**, *75*, 333–366.
4. Cherny, I.; Gazit, E. Amyloids: Not Only Pathological Agents but Also Ordered Nanomaterials. *Angew. Chem., Int. Ed.* **2008**, *47*, 4062–4069.
5. Kellermayer, M. S. Z.; Karsai, A.; Benke, M.; Soos, K.; Penke, B. Stepwise Dynamics of Epitaxially Growing Single Amyloid Fibrils. *Proc. Natl. Acad. Sci. U.S.A.* **2008**, *105*, 141–144.
6. Kowalewski, T.; Holtzman, D. M. *In-Situ* Atomic Force Microscopy Study of Alzheimer's β-Amyloid Peptide on Different Substrates: New Insights into Mechanism of β-Sheet Formation. *Proc. Natl. Acad. Sci. U.S.A.* **1999**, *96*, 3688–3693.
7. Hoyer, W.; Cherny, D.; Subramaniam, V.; Jovin, T. M. Rapid Self-Assembly of α-Synuclein Observed by *In-Situ* Atomic Force Microscopy. *J. Mol. Biol.* **2004**, *340*, 127–139.
8. Yang, H.; Fung, S. Y.; Pritzker, M.; Chen, P. Surface-Assisted Assembly of an Ionic-Complementary Peptide: Controllable Growth of Nanofibers. *J. Am. Chem. Soc.* **2007**, *129*, 12200–12210.
9. Whitehouse, C.; Fang, J. Y.; Aggeli, A.; Bell, M.; Brydson, R.; Fishwick, C. W. G.; Henderson, J. R.; Knobler, C. M.; Owens, R. W.; Thomson, N. H.; *et al.* Adsorption and Self-Assembly of Peptides on Mica Substrates. *Angew. Chem., Int. Ed.* **2005**, *44*, 1965–1968.
10. Zhang, F.; Du, H. N.; Zhang, Z. X.; Ji, L. N.; Li, H. T.; Tang, L.; Wang, H. B.; Fan, C. H.; Xu, H. J.; Zhang, Y.; *et al.* Epitaxial Growth of Peptide Nanofilaments on Inorganic Surfaces: Effects of Interfacial Hydrophobicity/Hydrophilicity. *Angew. Chem., Int. Ed.* **2006**, *45*, 3611–3613.
11. Du, H. N.; Li, H. T.; Zhang, F.; Lin, X. J.; Shi, J. H.; Shi, Y. H.; Ji, L. N.; Hu, J.; Lin, D. H.; Hu, H. Y. Acceleration of α-Synuclein Aggregation by Homologous Peptides. *FEBS Lett.* **2006**, *580*, 3657–3664.
12. Yang, G.; Woodhouse, K. A.; Yip, C. M. Substrate-Facilitated Assembly of Elastin-Like Peptides: Studies by Variable-Temperature *In Situ* Atomic Force Microscopy. *J. Am. Chem. Soc.* **2002**, *124*, 10648–10649.
13. Brown, C. L.; Aksay, I. A.; Saville, D. A.; Hecht, M. H. Template-Directed Assembly of a *De Novo* Designed Protein. *J. Am. Chem. Soc.* **2002**, *124*, 6846–6848.
14. Marsh, R. E.; Corey, R. B.; Pauling, L. An Investigation of the Structure of Silk Fibroin. *Biochim. Biophys. Acta* **1955**, *16*, 1–34.
15. Sunde, M.; Serpell, L. C.; Bartlam, M.; Fraser, P. E.; Pepys, M. B.; Blake, C. C. Common Core Structure of Amyloid Fibrils by Synchrotron X-ray Diffraction. *J. Mol. Biol.* **1997**, *273*, 729–739.
16. Cygan, R. T.; Liang, J. J.; Kalinichev, A. G. Molecular Models of Hydroxide, Oxyhydroxide, and Clay Phases and the Development of a General Force Field. *J. Phys. Chem. B* **2004**, *108*, 1255–1266.
17. Kuwahara, Y. Muscovite Surface Structure Imaged by Fluid Contact Mode AFM. *Phys. Chem. Miner.* **1999**, *26*, 198–205.
18. Osman, M. A.; Suter, U. W. Determination of the Cation-Exchange Capacity of Muscovite Mica. *J. Colloid Interface Sci.* **2000**, *224*, 112–115.
19. Nock, S.; Spudich, J. A.; Wagner, P. Reversible, Site-Specific Immobilization of Polyarginine-Tagged Fusion Proteins on Mica Surfaces. *FEBS Lett.* **1997**, *414*, 233–238.
20. Cheng, L.; Fenter, P.; Nagy, K. L.; Schlegel, M. L.; Sturchio, N. C. Molecular-Scale Density Oscillations in Water Adjacent to a Mica Surface. *Phys. Rev. Lett.* **2001**, 87.
21. Xu, K.; Cao, P.; Heath, J. R. Graphene Visualizes the First Water Adlayers on Mica at Ambient Conditions. *Science* **2010**, *329*, 1188–1191.
22. Odelius, M.; Bernasconi, M.; Parrinello, M. Two Dimensional Ice Adsorbed on Mica Surface. *Phys. Rev. Lett.* **1997**, *78*, 2855–2858.
23. Knowles, T. P.; Fitzpatrick, A. W.; Meehan, S.; Mott, H. R.; Vendruscolo, M.; Dobson, C. M.; Welland, M. E. Role of Intermolecular Forces in Defining Material Properties of Protein Nanofibrils. *Science* **2007**, *318*, 1900–1903.
24. Serpell, L. C. Alzheimer's Amyloid Fibrils: Structure and Assembly. *Biochim. Biophys. Acta* **2000**, *1502*, 16–30.
25. Liu, P.; Huang, X.; Zhou, R.; Berne, B. J. Observation of a Dewetting Transition in the Collapse of the Melittin Tetramer. *Nature* **2005**, *437*, 159–162.

26. Zhou, R. Trp-Cage: Folding Free Energy Landscape in Explicit Water. *Proc. Natl. Acad. Sci. U.S.A.* **2003**, *100*, 13280–13285.
27. Zhou, R.; Huang, X.; Margulis, C. J.; Berne, B. J. Hydrophobic Collapse in Multidomain Protein Folding. *Science* **2004**, *305*, 1605–1609.
28. Zhang, F. C.; Zhang, F.; Su, H. N.; Li, H.; Zhang, Y.; Hu, J. Mechanical Manipulation Assisted Self-Assembly To Achieve Defect Repair and Guided Epitaxial Growth of Individual Peptide Nanofilaments. *ACS Nano* **2010**, *4*, 5791–5796.
29. Loewenstein, W. The Distribution of Aluminum in the Tetrahedra of Silicates and Aluminates. *Am. Mineral.* **1954**, *39*, 92–96.
30. Brigatti, M. F.; Guggenheim, S. Mica Crystal Chemistry and the Influence of Pressure, Temperature, and Solid Solution on Atomistic Models. In *Micas: Crystal Chemistry and Metamorphic Petrology*; Mottana, A., Sassi, F. P., Thompson, J. B., Jr., Guggenheim, S., Eds; Mineralogical Society of America: Washington, DC, 2002; Vol. 46, pp 1−97.
31. MacKerell, A. D.; Bashford, D.; Bellott, M.; Dunbrack, R. L.; Evanseck, J. D.; Field, M. J.; Fischer, S.; Gao, J.; Guo, H.; Ha, S.; *et al.* All-Atom Empirical Potential for Molecular Modeling and Dynamics Studies of Proteins. *J. Phys. Chem. B* **1998**, *102*, 3586–3616.
32. Jorgensen, W. L.; Chandrasekhar, J.; Madura, J. D.; Impey, R. W.; Klein, M. L. Comparison of Simple Potential Functions for Simulating Liquid Water. *J. Chem. Phys.* **1983**, *79*, 926–935.
33. Phillips, J. C.; Braun, R.; Wang, W.; Gumbart, J.; Tajkhorshid, E.; Villa, E.; Chipot, C.; Skeel, R. D.; Kale, L.; Schulten, K. Scalable Molecular Dynamics with Namd. *J. Comput. Chem.* **2005**, *26*, 1781–1802.
34. Kumar, S.; Huang, C.; Zheng, G.; Bohm, E.; Bhatele, A.; Phillips, J. C.; Yu, H.; Kale, L. V. Scalable Molecular Dynamics with Namd on the IBM Blue Gene/L System. *IBM J. Res. Dev.* **2008**, *52*, 177–188.
35. Darden, T.; York, D.; Pedersen, L. Particle Mesh Ewald: An *N*log(*N*) Method for Ewald Sums in Large Systems. *J. Chem. Phys.* **1993**, *98*, 10089–10092.